energies

MDPI

Article

Solidification of Graphene-Assisted Phase Change Nanocomposites inside a Sphere for Cold Storage Applications

Rajendran Prabakaran [1], Shaji Sidney [1], Dhasan Mohan Lal [1,*], C. Selvam [2] and Sivasankaran Harish [3,*]

1 Department of Mechanical Engineering, Anna University, College of Engineering Campus, Chennai 600 025, India
2 Department of Mechanical Engineering, SRM Institute of Science and Technology, Chennai 603 203, India
3 International Institute for Carbon-Neutral Energy Research, Kyushu University, Nishi-ku, Fukuoka 819-0395, Japan
* Correspondence: mohanlal@annauniv.edu (D.M.L.); harish@i2cner.kyushu-u.ac.jp (S.H.); Tel.: +91-44-22357609 (D.M.L.); +81-92-802-6730 (S.H.)

Received: 15 August 2019; Accepted: 6 September 2019; Published: 9 September 2019

Abstract: In this work, we experimentally investigated the solidification behavior of functionalized graphene-based phase change nanocomposites inside a sphere. The influence of graphene nanoplatelets on thermal transport and rheological characteristics of the such nanocomposites were also discussed. We adopted the covalent functionalization method to prepare highly stable phase change nanocomposites using commercially available phase change material (PCM) OM08 as the host matrix and graphene nanoplatelets (GnPs) with 0.1, 0.3, and 0.5 volume percentage as the nano inclusions. We report a maximum thermal conductivity enhancement of ~102 and ~46% with 0.5 vol% in the solid and liquid states, respectively. Rheological measurements show that the pure PCM shows Newtonian behavior, whereas the inclusion of GnPs leads to the transition to non-Newtonian behavior, especially at lower shear rates. Viscosity of the nanocomposite increases with an increase in the volume fraction of GnP. For 0.5 vol% of GnPs, maximum increase in viscosity was found to be ~37% at a shear rate of 1000 s^{-1}. Time required for complete solidification decreases with the loading of GnPs. Maximum reduction in solidification time with 0.5 vol% of GnPs was ~40% for bath temperature of −10°C.

Keywords: solidification; phase change material; fatty acids; graphene nanoplatelets; cold thermal energy storage

1. Introduction

In recent years, air conditioning systems in vehicles have received great attention due to ozone depletion and NOx emission issues. The automobile sector contributes to 23% of overall greenhouse emissions [1] and the usage of air conditioners is also a major factor, which consumes 12–17% of the total engine power [2]. An attempt has been made to reduce the fuel consumption and greenhouse gas emissions from engines during traffic periods by using the start/stop (S/S) technology in vehicles [3]. The use of start/stop technology in small-sized cars could reduce CO_2 emission by 20% [4]. The engine gets switched off during the traffic time for a longer period with the use of start/stop technology, and the compressor of an air conditioner stops running. This could affect the thermal comfort of the passengers in the cabin and raise the cabin temperature due to the penetration of heat from outside, especially in urban areas. To overcome this problem, a thermal energy storage system (TES) could be a possible solution in the mobile air conditioning system (MAC) as a secondary cooling coil. The TES

system can store cold energy when the air conditioner runs and subsequently serve cold energy to the passenger cabin during the start/stop period.

The TES system plays a significant role in storing thermal energy in building air conditioning, solar energy, waste heat recovery, etc. It is also used as an excellent energy-saving technique in air conditioning applications. Latent heat based TES systems (LHTES) are promising owing to their high energy storage density, isothermal energy storage and release [5]. Many phase change materials (PCM) are used in LHTES systems, such as paraffins, salt hydrates, organic alkanes, alkeones, fatty acids, and eutectic mixtures. Among these, fatty acid-based PCMs are best suited for energy storage, especially for temperature conditions below the ambient temperature. They possess good thermo-physical properties such as high energy storage density, low cost, no subcooling, being non-toxic, having corrosive resistance, high thermal stability, and with the low volume change during phase transition [6].

Bista et al. [7] experimentally evaluated PCM TES inclusion on the performance of vapor compression refrigeration system, compressor cycling, and annual energy consumption. The PCM was placed in the evaporator/condenser side and food compartment individual and its effects were analyzed. They found that the addition of the PCM in the evaporator side increased the initial compressor cut in cycle and condenser temperature, while the condenser pressure and energy consumption were reduced with the PCM in the condenser side. However, the compressor cycling was not uniformed and it required more displacement with the condenser side PCM. The position of the PCM-based TES in the food compartment also resulted in a marginal drop in coefficient of performance (COP).

Elarem et al. [8] carried out the effect of integrated PCM slabs with evaporator compartment on the COP and energy consumption of the refrigerator. The commercial A4 (PluseICE) organic PCM with a phase transition temperature of 4 °C was used. They reported that the system COP was increased by 12%, with 8% reduction in energy consumption. Maiorino et al. [9] and Bakhshipour et al. [10] also reported similar results with integration of PCMs in the refrigerator. Yamada et al. [11] developed and tested the cold TES evaporator in a MAC system for stop/start vehicles to extend the thermal comfort during traffic waiting periods. The results showed that cabin comfort was extended up to 19 and 38 s with conventional and TES evaporators, respectively, while the average fuel consumption was dropped by up to 7.5% with TES evaporator. Wang et al. [12] found that the PCM heat exchanger with a capacity of 0.45 kWh and 33 kg of PCM improved the electrical vehicle running time by 20%, while maintaining thermal comfort in the cabin. From the previous studies, it was found that the utilization of PCM TES had lower energy consumption and CO_2 emission in the commercial, passenger and transport air conditioning, and refrigeration applications.

However, limited thermal conductivity of the PCMs is unfavorable for the enhancement of system performance with TES [13]. The energy storage process mainly depends on the conduction heat transfer of the PCM after solidification starts, and therefore it is necessary to enhance the thermal conductivity of the PCM to enhance the system performance. There are many methods proposed to improve the thermal conductivity of the PCMs. Recent literature shows that the addition of nanomaterials significantly enhances the thermal conductivity of PCMs [14]. Many nanomaterials such as Al_2O_3, SiO_2, CuO, carbon nanohorns, single-walled carbon nanotubes, multi-walled carbon nanotubes, graphene nanoplatelets (GnPs), expanded graphite and carbon nanofibers, etc., were investigated by the researchers to increase the thermal conductivity and heat transfer rate. Among these, GnPs have excellent potential to enhance the thermal conductivity to a higher level because of their two-dimensional planar structure [15–18]. The problem associated with the utilization of GnPs is agglomeration and sedimentation over the course of time. This can be reduced by adding the surfactant (non-covalent functionalization methods) in the nanocomposites. However, the inclusion of the surfactant may reduce the specific heat with higher viscosity, and these two conflicting effects may affect the energy storage/release process [19]. In regard to this, chemical treatment of GnPs (covalent functionalization) could be a better option. In this technique, concentrated nitric acid treatment was adopted to modify the surface of GnPs to increase the number of surface-active sites for electrochemical reactions due to the hydrophobic tendency of GnPs. The number of oxygen/nitrogen-containing

functional groups formed on the surface of the graphene increased after acid treatment and thus, it increased the hydrophilicity of GnPs [20]. Moreover, studies on the rheological behavior of the PCM nanocomposites are limited in literature [21].

It is essential to analyze the effects of nanoparticles on PCM solidification and melting processes in a container before using it in the practical TES systems. This gives a good understanding of the energy storage/release behavior of nanocomposites. Recent studies on carbon-based nanocomposites for cold TES are tabulated in Table 1. Sathishkumar et al. [22] studied the solidification of water-based GnP nanocomposite in a spherical capsule and observed that the solidification time was reduced by 25% with 1.2 mass % of GnPs. Sidney et al. [20] experimentally analyzed the solidification and melting of water-based GnP composite in a cylindrical container. They used functionalized GnPs instead of using surfactants for improving the thermal stability. It was found that the addition of GnPs reduced the solidification time by 43% and 32% for the bath temperatures of −6 °C and −10 °C, respectively, with 0.5 vol% of GnPs.

Table 1. Recent studies on the solidification of PCM nanocomposites with carbon-based nanomaterials for cold TES application.

Authors	Phase Change Material	Nanomaterial	Observation
Sidney et al. [20]	Deionized water	Functionalized GnPs	Solidification time of GnP nanocomposite with 0.5 vol% of GNPs was decreased by 43% and 32% for bath temperatures of −6 °C and −10 °C, respectively.
Sathishkumar et al. [22]	Deionized water	GnPs	Solidification time decreased by 21% and 25% at bath temperatures of −9 °C and −12 °C, respectively, with 0.5 vol% of GnPs.
Kumaresan et al. [23]	Paraffin (RT 20)	MWCNT	With 0.6 vol% of MWCNT, the solidification time of PCM nanocomposite decreased by 33.64%.
Kumaresan et al. [24]	Deionized water	MWCNT	Solidification time decreased by 14% and 20% for the bath temperatures of −9 °C and −12 °C with 0.6 vol% of MWCNT inclusion.
Chandrasekaran et al. [25]	Deionized water	MWCNT	Freezing time was reduced by 25% with 0.1 wt% of MWCNT.
Liu et al. [26]	Deionized water	Graphene oxide	Solidification was shortened by 66% with 50 mg of GO in 100 ml water.
Mo et al. [27]	Deionized water	L-MWNT-1030	Solidification time was reduced from 4 h and 30 min to 3 h and 20 min.

In our previous study [28], melting behavior of the GnPs enhanced OM08 PCM in a sphere shows that the addition of GnPs reduced the melting time by up to 26% and 21% with 0.5 vol%. It was also found that the addition of GnPs led to transition from Newtonian to non-Newtonian behavior at low shear rates. Dynamic viscosity of such nanocomposite had a major impact on the melting behavior of the PCM nanocomposite. There was no significant reduction in the melting time between the GnP loadings of 0.4 and 0.5 vol%. Thus, the addition of GnPs was limited to 0.5 vol%. In this study, a miniature work was carried out using a spherical capsule to understand heat transfer phenomenon during solidification of PCM with GnP inclusion, before implementing it in the MAC system. Limited work has been done with GnP nanocomposites for cold TES, and no work has been reported using functionalized GnPs with fatty acids for cold TES. The novelty of this work is to study solidification behavior of the fatty acid-based PCM with GnPs inside a sphere for potential utilization in automobile air conditioning systems. Further, the effects of GnP addition on the thermal conductivity and rheological behavior were also analyzed. The experiment was performed for various bath temperatures (–10, 2, and 5 °C) and 0, 0.1, 0.3 and 0.5 vol% of GnP loadings.

2. Experimentation

2.1. Material Selection

The PCM was selected based on the operating temperature range of the particular application considered in this study. Air temperature leaving the MAC system's cooling coil is in the range of 3–16 °C [29]. So, in this study, we chose the PCM whose phase change temperature was at ~8 °C. For this application, commercially available fatty acid-based PCM OM08 with a phase change temperature of 8–9 °C was purchased from Pluss Technologies, India and its properties are shown in Table 2. PCM OM08 was selected due to its compatibility with aluminum, which is often used in MAC heat exchangers and has low volume change during phase transition (<5%). The grade M multilayered GnPs (diameter 25 μm, mean thickness of 5–10 nm, density of 2.2 g cm^{-3}) were purchased from XG Science (Lansing, MI, USA). The typical multilayer flake-shaped structure of the GnPs was confirmed by Scanning Electron Microscopy (SEM) (FEI 3d Versa Dual Beam, HillsBro, Oregon, USA), as shown in Figure 1.

Table 2. Thermo-physical Properties of OM 08.

Property	Value [a]
Phase change temperature	8–9 °C
Density (liquid phase) ρ_l (at 30 °C)	1050 kg m^{-3}
Density (solid phase) ρ_s (at 0 °C)	1111 kg m^{-3}
Thermal conductivity (liquid phase) k_l (at 30 °C)	0.168 W m^{-1} K^{-1}
Thermal conductivity (Solid phase) k_s (at –5 °C)	0.235 W m^{-1} K^{-1}
Latent heat h (0–9 °C)	180 kJ kg^{-1}
Specific heat (liquid phase) c_{pl} (30 °C)	2.1 kJ kg^{-1} K^{-1}
Specific heat (solid phase) c_{ps} (0 °C)	1.71 kJ kg^{-1} K^{-1}
Flash point	110 °C

[a] http://www.pluss.co.in/technical-datasheets/Doc366-TDS-OM-08.pdf.

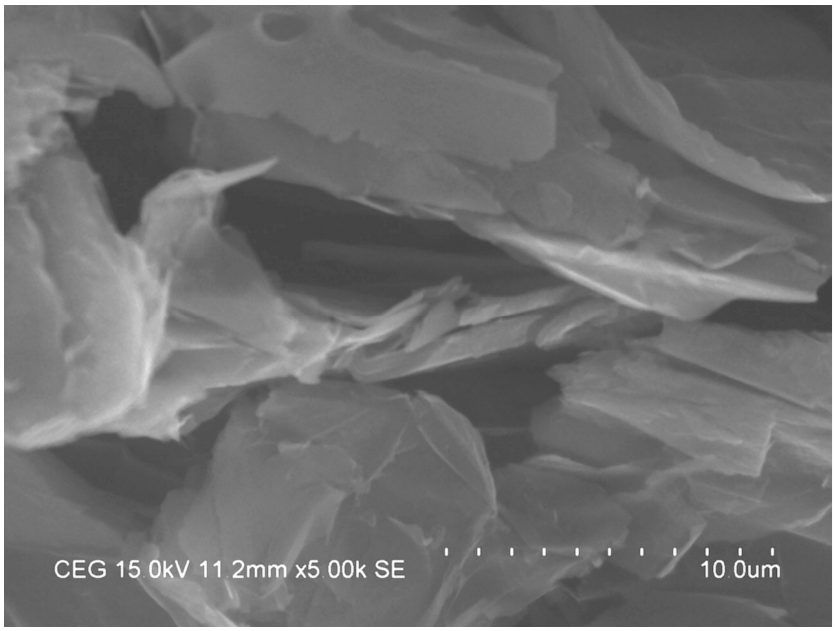

Figure 1. SEM visualization of graphene nanoplatelets (GnPs).

2.2. Functionalization of GnPs

At first, 10 g of GnPs was dispersed in 500 ml of concentrated nitric acid (65%). The mixture was heated and refluxed in oil bath at 100 °C for 2 h. The heated mixture was diluted in deionized water until the PH value became 7 and then the GnP flakes were filtered. Filtered GnPs were kept in a furnace for 8 h at 160 °C to remove the moisture content.

2.3. Preparation of PCM Nanocomposites

The required amount of functionalized GnPs (0.1 vol%) was dispersed in liquid PCM using a hot plate type magnetic stirrer at a temperature of 35 °C at 350 rpm for a time of 30 min. Following this, the sample was sonicated at a frequency of 30 GHz for 90 min by using a digital sonicator (QSonica, USA). The same procedure was repeated to prepare the PCM nanocomposites of different loadings with functionalized GnPs (0.3 and 0.5 vol%). The prepared samples were kept undisturbed for 10 days and it was confirmed visually that there was no settlement of GnPs. Further, the stability of nanocomposite was measured by the zeta potential distribution method, which was previously reported in our work [28].

2.4. Experimental Facility

The experimental setup, as previously reported in our work on melting [28], consisted of a spherical capsule (made: Aluminum, outer diameter: 80 mm), a constant temperature refrigerating bath (Capacity: 5 l), cooling coil, temperature controller and data logging unit (Agilent-34970A) with a personal computer, as shown in Figure 2. Generally, freezing inside the sphere is symmetric about its vertical axis when the surrounding is maintained at a constant temperature. To understand the solidification behavior of the PCM, we placed resistance temperature detectors (RTDs) at five different locations in the spherical capsule, as shown in Figure 3. A mixture of ethylene glycol and water (ratio of 40:60 by volume) was used as the heat transfer fluid (HTF) in the refrigerating bath. The temperature of the bath was controlled by a proportional integral derivative controller (PIDC) and an electrically-driven stirrer was used to maintain constant temperature in the bath. The cooling bath was completed insulted using polyurethane form to reduce the heat losses.

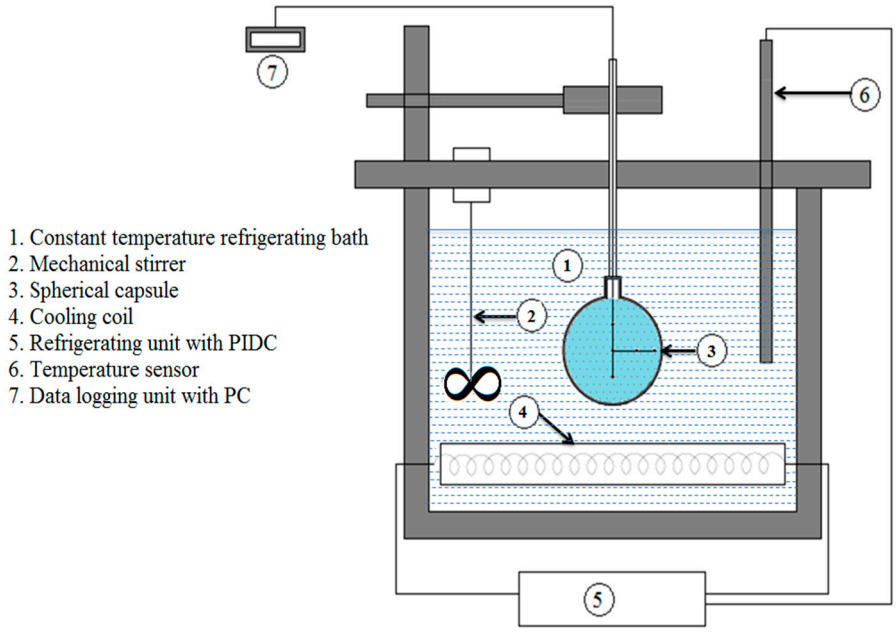

Figure 2. Schematic representation of the experimental setup [28].

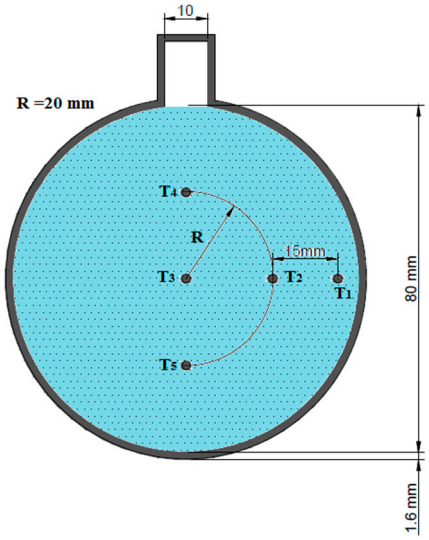

Figure 3. Schematic of the spherical capsule with the locations of the temperature sensors [28].

2.5. Experimental Procedure

The refrigeration unit, along with the stirrer motor, was switched ON and the required bath temperature of −10 °C was fixed by using the temperature controller. Once the required bath temperature was attained, the controller regulated the power supply to the cooling coil to maintain a constant temperature. The PCM nanocomposite was filled in the capsule up to 90% of its volume and then was heated to 31 °C using a separate bath. After attaining uniform temperature throughout the capsule, it was then immersed in the refrigerating bath and this initiated the solidification process of the PCM nanocomposite. The temperatures of the PCM nanocomposite at various locations in the capsule were logged into the computer with a time interval of 10 s, until thermal equilibrium was attained. Then, the same procedure was repeated for the PCM nanocomposite for the different bath temperatures of 2 °C and 5 °C and the remaining vol% of GnPs (0.3 and 0.5 vol%).

2.6. Measurement of Thermal Conductivity and Rheological Behavior

We used KD2 Pro thermal property analyzer (Decagon Devices, USA) to measure the thermal conductivity in this work. The KS1 sensor measures the thermal conductivity with an accuracy of ±5%. Thermal conductivity of the PCM nanocomposites was measured at the solid and liquid states based on the method adopted by Sidney et al. [20]. Thermal conductivity measurements were performed at least 10 times at a particular temperature to confirm repeatability. Rheological measurements were performed using Anton Paar MCR 302 rheometer for a shear rate range of 1–1000 s^{-1} at ambient temperature.

Uncertainty of the solidification time ($t_{solidification}$) and the total experiment (E_{total}) were estimated as reported by Moffat [30], which is described below:

$$\frac{\partial x}{x} = \sqrt{\left(\frac{\partial x_1}{x_1}\right)^2 + \left(\frac{\partial x_2}{x_2}\right)^2 + \ldots..\left(\frac{\partial x_n}{x_n}\right)^2} \quad (1)$$

The total solidification time ($t_{solidification}$) is a function of the mass of the PCM filled in the capsule ($\dot{m}_{PCM}$) bath temperature (T_{bath}), initial temperatures of the PCM ($T_{PCM,initial}$), final temperatures of the PCM ($T_{PCM,final}$), and data logging ($t_{data,logger}$). Similarly for the total experiment (E_{total}) is a function of the total solidification time ($t_{solidification}$), thermal conductivity (k_{pcm}), and viscosity (μ_{pcm}) of the PCM.

$$t_{solidification} = f\left[\dot{m}_{PCM}, T_{PCM,initial}, T_{bath}, T_{PCM,final} \;\&\; t_{data,logger}\right] \quad (2)$$

$$\frac{\partial t_{solidification}}{t_{solidification}} = \left[\left(\frac{\partial m_{pcm}}{m_{pcm}}\right)^2 + \left(\frac{\partial T_{pcm,initial}}{T_{pcm,initial}}\right)^2 + \left(\frac{\partial T_{pcm,final}}{T_{pcm,final}}\right)^2 + \left(\frac{\partial T_{bath}}{T_{bath}}\right)^2 + \left(\frac{\partial t_{bath\ logger}}{t_{bath\ logger}}\right)^2\right]^{0.5} \quad (3)$$

$$\frac{\partial E_{total}}{E_{total}} = \left[\left(\frac{\partial t_{solidification}}{t_{solidification}}\right)^2 + \left(\frac{\partial k_{pcm}}{k_{pcm}}\right)^2 + \left(\frac{\partial \mu_{pcm}}{\mu_{pcm}}\right)^2\right]^{0.5} \quad (4)$$

Uncertainties for the time of solidification and total experiment were estimated as ±2.3% and ±5.9%, respectively.

3. Results and Discussion

In this section, the effect of functionalized GnPs on the thermal conductivity and rheological behavior are discussed. The solidification behavior of the nanocomposites for varying GnP loadings at different bath temperatures is also discussed in detail.

3.1. Effect of GnP Loading on the Thermal Conductivity of PCM Nanocomposites

The effect of functionalized GnPs on the thermal conductivity of nanocomposites for the temperature range of −20 to 40 °C is shown in Figure 4. The measured thermal conductivity of pure PCM at 30 °C and −10 °C was in good agreement with the manufacturer data, shown in Table 1, within a range of ±5%. As seen from Figure 4, the inclusion of GnPs in the PCM increases the thermal conductivity of the nanocomposites and decreases with temperature. It is also observed that there is a sudden increase in thermal conductivity in the liquid to solid phase transition region, and it attains maximum thermal conductivity after complete solidification. Maximum enhancement in thermal conductivity for the 0.5 vol% of GnPs is found to be 102.17% and 45.69% in solid and liquid states, respectively.

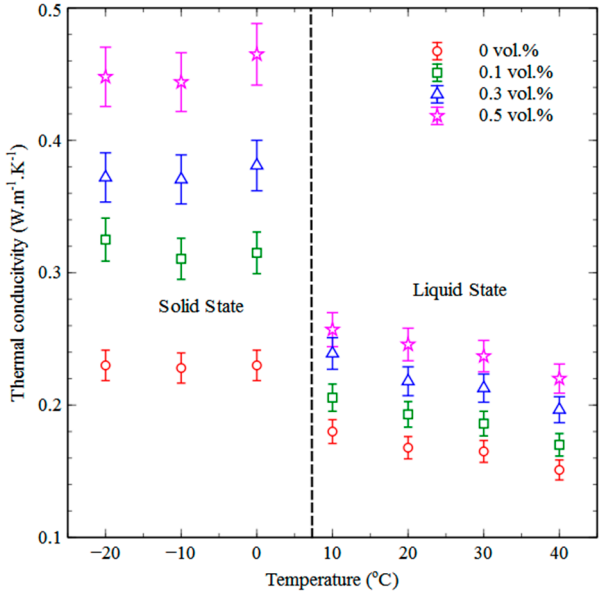

Figure 4. Effect of functionalized GnP loading and temperature on the thermal conductivity of the PCM nanocomposites.

The reason behind the higher thermal conductivity enhancement in the solid state than that in the liquid is attributed to the formation of percolating networks formed during the phase transition and the crystalline nature in the solid state which minimizes the interfacial resistance [28,31]. The lower enhancement in the liquid phase of the nanocomposite is attributed to the molecular disorder of the PCM during phase transition and higher interfacial resistance [31,32]. Harish et al. [32] also reported that the thermal conductivity enhancement of PCM with 1% of GnP loading in solid and liquid states

were 223% and 37%, respectively. It is also observed from Figure 4 that the variation of solid state thermal conductivity with respect to temperature is not significantly changed.

3.2. *Effect of GnP Loading on Rheological Behavior of the PCM Nanocomposites*

The effect of GnP loading and the shear rate on the dynamic viscosity and shear rate of PCM nanocomposites at 20 °C is shown in Figure 5. It indicates that the inclusion of GnPs increases the dynamic viscosity of the PCM nanocomposites, whereas it reduces with the shear rate because of the shear thinning behavior. The rheological characteristics of the fluid is classified into two types—as Newtonian and non-Newtonian. If the viscosity of the fluid does not change with shear stress, it is said to be Newtonian, while if it is a changes with shear stress, it is classified as non-Newtonian fluid [33].

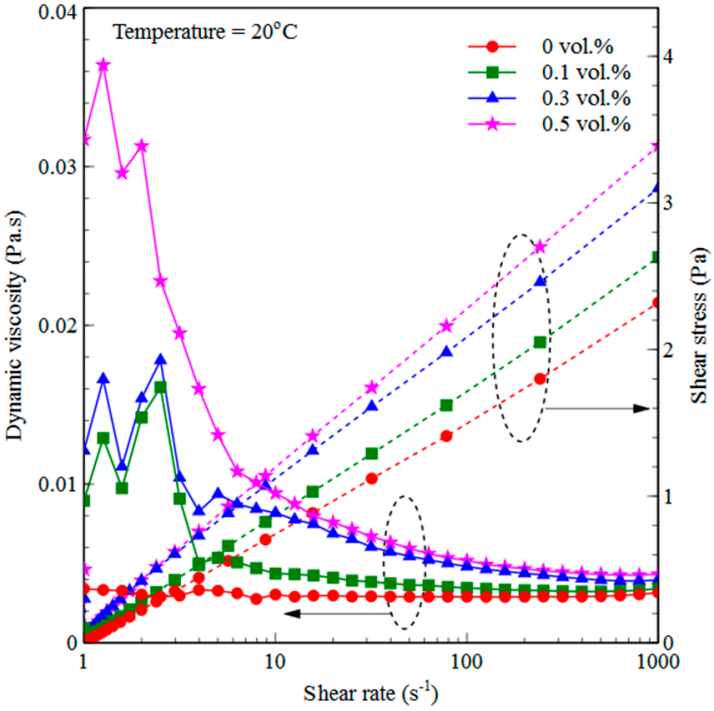

Figure 5. Effect of GnP loadings and shear rate on dynamic viscosity and shear stress of the PCM nanocomposites at 20 °C.

As seen from Figure 5, the viscosity of the pure PCM composite does not change with shear rate and it clearly indicates Newtonian behavior. However, viscosity of the nanocomposites varies with respect to shear rate of 1–200 s^{-1} and further increase in shear rate does not alter the viscosity. This shows the non-Newtonian behavior of PCM nanocomposites at low shear rates. Parameshwaran et al. [21] and Kumaresan et al. [23] also reported similar rheological behavior with PCM nanocomposites. The maximum increase in dynamic viscosity of the PCM nanocomposite is found to be 37.02% with 0.5 vol% of GnPs at a shear rate of 1000 s^{-1}.

As seen from Figure 5, the shear stress of the pure PCM linearly increases with shear rate, while the addition of GnPs lead to a non-linear increase in shear stress at lower shear rates for the PCM nanocomposites. These results also confirm the Newtonian behavior of pure PCM and non-Newtonian behavior of PCM nanocomposites. It is inferred that the addition of GnPs could cause the natural convection predominantly at low shear rates in the liquid phase during solidification due to the increased dynamic viscosity, while the increased thermal conductivity helps to enhance the heat transfer in both solid and liquid phases.

3.3. Solidification of Pure PCM in a Spherical Capsule

Solidification behavior of pure PCM at varying locations of T_1, T_2, T_3, T_4, and T_5 inside the spherical capsule at the bath temperatures of −10 °C is shown in Figure 6. During the initial stage of the solidification process, the temperature at all the measured locations drops quickly to 10 °C within 12 min. At this phase, the PCM is in liquid phase and heat transfer between the molecules of the PCM is completely dominated by the natural convection until solidification begins near the wall. This convective current allows better heat transfer between the molecules of the liquid PCM and heat transfer with the container wall, resulting in faster temperature drop at all the other locations.

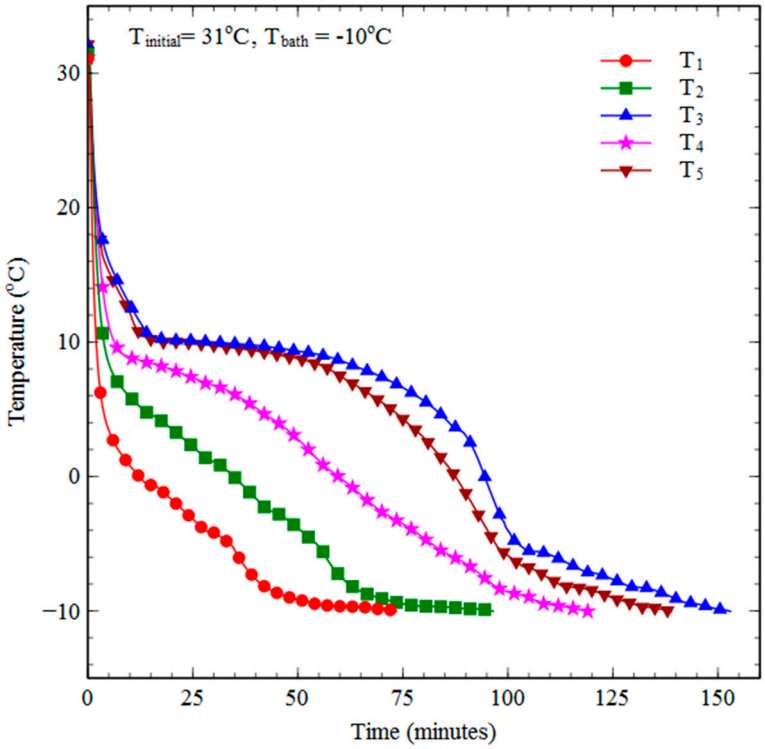

Figure 6. Temperature change at different locations as a function of time during solidification of pure PCM.

Once the temperature falls below 10 °C, the PCM starts solidifying and the solidification process is mainly dominated by the conduction heat transfer between the container wall and solid molecules of the PCM. Thus, temperature near the container wall at location T_1 drops quickly and that at T_3 decreases very slowly. The temperature at other locations T_2, T_4, and T_5 (R = 20 mm) are symmetric about the centre (T_3) and should exhibit similar temperature drops. However, the temperature drops quickly at T_2, followed by T_4 and T_5. This is because the solidified PCM tries to sink to the bottom of the capsule due to its high density, and the liquid molecules of the PCM move upward due to natural convection effects. The presence of temperature sensors inside the capsule prevents the downward motion of the solidified PCM as solidification commences on the surface of the sensors. Due of this phenomenon, the temperature drops at T_4 and T_5 are delayed by 22.5 and 37.5 min than that of T_2. Time taken for complete solidification at locations T_1, T_2, T_3, T_4, and T_5 is measured to be 73.5, 96.5, 153, 119, and 139 min, respectively. Li et al. [34] also reported similar trends of solidification behavior of paraffin-based PCM in a spherical container.

In practice, source temperature of the air conditioning unit is varied based on the cooling demand and other operational conditions. Therefore, it is very important to analyze the solidification behavior for different bath temperatures. The trend of drops in temperature at all the locations is the same as the bath temperature increases to 2 °C and 5 °C. The effects of bath temperature on the solidification

of pure PCM at the center of the capsule (T_3) are shown in Figure 7. It shows that the decrease in bath temperature decreases the solidification time of the pure PCM, owing to the higher potential of temperature drive. The time taken for complete solidification is found to be 153, 274, and 470 min at the bath temperatures of –10, 2, and 5 °C, respectively.

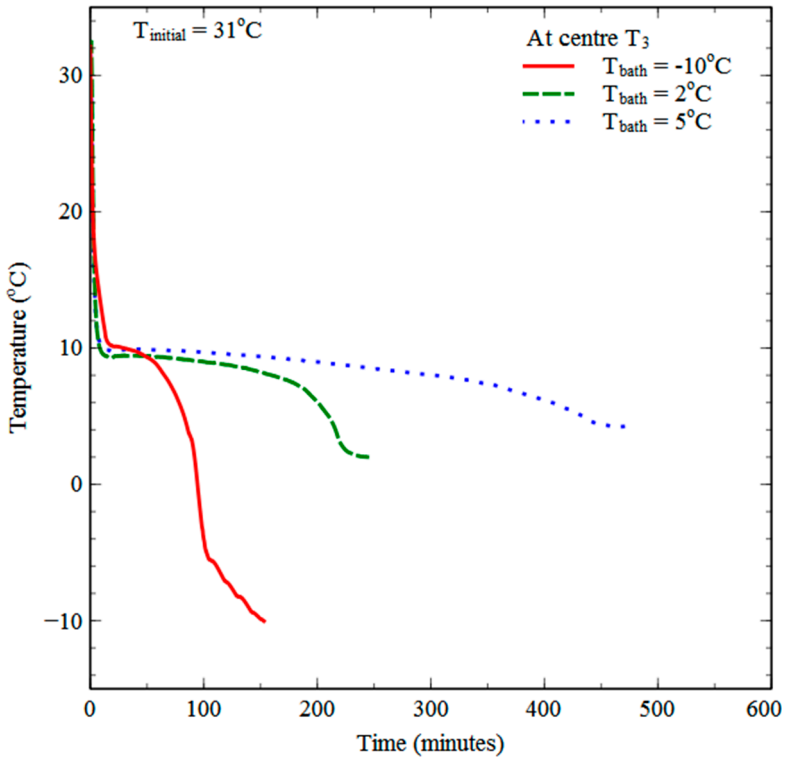

Figure 7. Effect of bath temperature on solidification of pure PCM at center (T_3) of the sphere.

3.4. Effect of GnP Loading on the Solidification Behavior of the PCM Nanocomposites

The effect of functionalized GnP loading with variation in temperature at the center (T_3) of the spherical capsule during solidification from 32 °C to −10 °C is shown in Figure 8. It shows that the drop in temperature is faster in both solid and liquid phases when the GnP volume percentage increases. This indicates that the increase in viscosity does not commensurate with higher thermal conductivity during the temperature drop in liquid phase. The time required to reach 10 °C at the center is found to be 29, 12, 10, and 9 min with 0, 0.1, 0.3, and 0.5 vol% of GnP loadings. It indicates that the drop in temperature during the liquid phase is found to be more significant with lower volume fraction of GnP (<0.1 vol%), and further addition of GnPs does not yield a significant drop in the time. This could be due to the higher dynamic viscosity with high volume fractions of GnPs that affects the natural convection between the liquid molecules of the PCM nanocomposites. Time required to attain a thermal equilibrium state of PCM nanocomposite at the centre (T_3) is found to be 153, 129, 113, and 93 min with 0, 0.1, 0.3, and 0.5 vol% of GnP loadings. The drop in solidification time is found to be 15.68, 26.14, and 39.21% with 0.1, 0.3, and 0.5 vol% of GnP loadings. Based on our previous studies [28], there was no significant reduction in melting time while increasing GnP loadings from 0.4 to 0.5 vol%, due to the increased dynamic viscosity. Thus, the study is limited to 0.5 vol% GnP concentration.

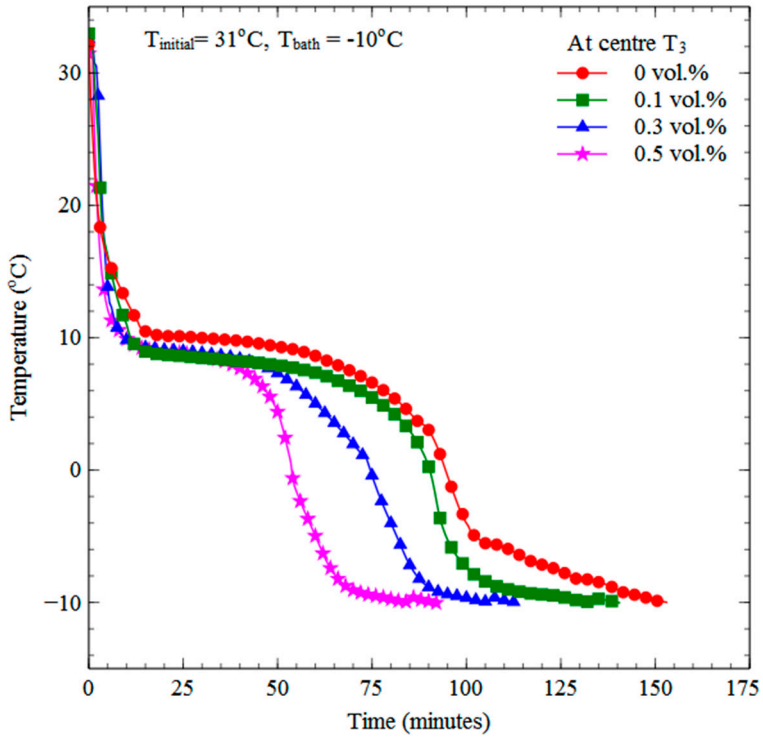

Figure 8. Effect of GnP loadings on the temperature variation at center (T_3) during solidification.

Time taken for solidification to complete for the PCM nanocomposites at different locations in the capsule for the various volume fractions of GnPs is shown in Figure 9. It shows that the solidification time reduces at all the measured locations with increase in GnP concentration. At first, the PCM nanocomposite solidifies at the location T_1, followed by the locations T_2, T_4, T_5, and T_3. The same solidification trend was experienced with the pure PCM, as shown in Figure 6. The maximum drop in solidification at locations T_1, T_2, T_4, and T_5 is found to be 52.4, 34.7, 30, and 37.7%, respectively.

When comparing to other locations, the reduction in solidification is superior at location T_1; this could be due to quicker sensible cooling and direct contact between the capsule wall and the PCM layer. When compared to the other locations, the percentage reduction in solidification time at locations T_2 and T_4 are lower. This is attributed to the increase in dynamic viscosity of the nanocomposite, which suppresses the free-flow motion of the fluid molecules, particularly at the surface of GnPs, which affects the natural convention and slows down the movement of the PCM liquid molecules from the top to the bottom of the capsule and vice versa. The overall effect of the above phenomenon affects the temperature profile at locations T_2 and T_4 in the capsule.

The solidification process mainly depends on the source temperature (air conditioning application). Generally, the cooling coil temperature varies based on the various operating parameters. The effects of bath temperature and GnP loading on the solidification time are shown in Figure 10. The solidification time increases with the increase in bath temperature and decreases with GnP loading. For pure PCM, solidification time is delayed by 78% and 205% when the bath temperature is increased from −10 °C to 2 °C and 5 °C, respectively. The time delay increases as the GnP volume percentage increases. At 0.5 vol%, the solidification process is delayed by 114% and 228% when the bath temperature is varied from −10 °C to 2 °C and 5 °C, respectively. Maximum reduction in solidification time of the PCM nanocomposite with 0.5 vol% of GnPs is found to be 39.21, 32.48, and 30.85% when the bath temperatures are −10, 2, and 5 °C, respectively. Overall, the reduction in solidification time due to the addition of GnPs is based on the accelerated energy storage due to the increased thermal conductivity of the PCM nanocomposites for the same PCM volume in the capsule.

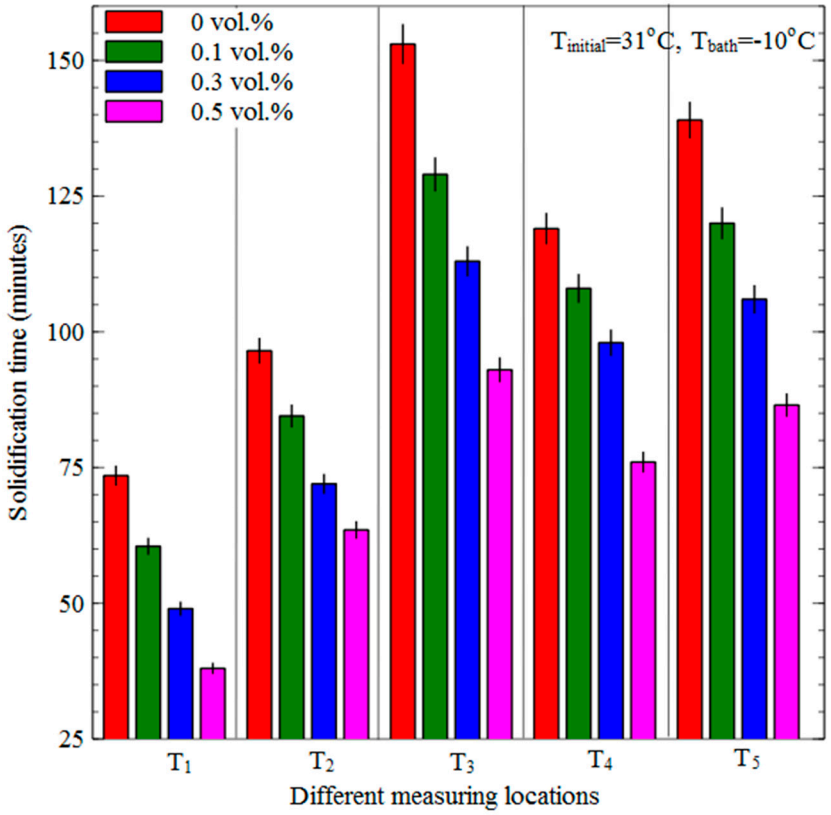

Figure 9. Solidification time of the PCM nanocomposites at different locations inside the sphere.

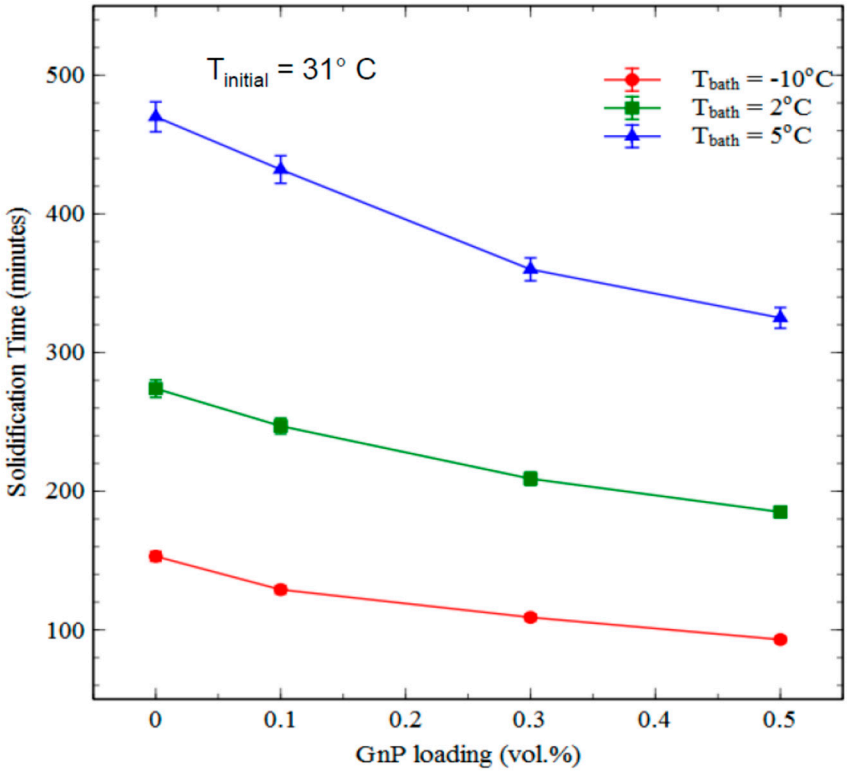

Figure 10. Solidification time of the PCM nanocomposites for various bath temperatures.

Comparison of the complete solidification time with the previously reported melting time [28] of the PCM nanocomposite for various GnP loadings is shown in Table 3. The solidification and melting time decreases with increase in temperature difference between the bath and PCM. For all the nanocomposites, the time required for complete solidification is higher than that of the melting time for the same temperature between the bath and the PCM. This phenomenon indicates that the solidification process is dominated by conduction heat transfer (more resistance), while the melting process is dominated by convection. The addition of GnPs has a higher percentage reduction in solidification time than that of the melting time for the same temperature difference between the bath and the PCM. Therefore, it is inferred that the increase in dynamic viscosity has more impact on the melting process than that of the solidification process.

Table 3. Comparison of complete solidification and melting timing of PCM nanocomposite for various GnP loading.

Volume Fraction of GnP (%)	Complete Solidification Time (minutes)		Complete Melting Time (minutes) [28]	
	31 to 2 °C	31 to −10 °C	2 to 31 °C	−10 to 31 °C
0	274	154	35.5	44
0.1	247	129	34	41.5
0.3	209	109	29	34.5
0.5	180	84	25.5	30

4. Conclusions

In this study, we experimentally show that the low concentration of graphene nanoplatelets significantly enhances the solidification rate inside a sphere, owing to the higher thermal conductivity enhancement, and we also report the heat transfer mechanism and PCM flow inside a spherical encapsulation. The solidification behavior of fatty acid-based (OM 08) PCM nanocomposites with functionalized GnPs inside a sphere was experimentally investigated. The effect of GnP loading on thermal conductivity and rheological behavior of the PCM nanocomposites was also investigated. Maximum enhancement in thermal conductivity of the PCM nanocomposite with 0.5 vol% of GnPs was found to be ~46% and ~102% in liquid and solid states, respectively. Rheological measurements show that pure PCM has Newtonian behavior, whereas the inclusion of GnPs results in the transition of Newtonian to non-Newtonian behavior at lower shear rates.

The initial solidification process is dominated by convection heat transfer and the conduction heat transfer plays the major role when solidification begins. The time required for complete solidification of the pure PCM was found to be 470, 274, and 153 min for the bath temperatures of 5, 2, and −10 °C, respectively. Maximum reduction in solidification time of the PCM nanocomposite with 0.5 vol% of GnPs was found to be ~31, ~32, and ~39% for bath temperatures of 5, 2, and −10 °C, respectively. These results could be very helpful to design and develop an efficient cold TES with low volume concentration of graphene nanoplatelets, which could make the climate control in vehicles more eco-friendly.

Author Contributions: Conceptualization, S.H. and D.M.L; methodology, R.P. and S.S.; formal analysis, R.P., S.S., S.C., and S.H; writing—original draft preparation, R.P.; writing—review and editing, S.S., S.H., and D.M.L; supervision D.M.L.

Funding: R.P. acknowledges the Centre for Research, Anna University for providing Anna Centenary Research Fellowship (ACRF) (Ref No.CFR/ACRF/2015/4, Dated 21.01.2015) for the doctoral level research. S.H. acknowledges the support of the International Institute for Carbon-Neutral Energy Research (WPI-I2CNER).

Conflicts of Interest: The authors declare no conflict of interest.

Nomenclature

Abbreviation	
GnPs	Graphene nanoplatelets
LHTES	Latent heat thermal energy storage
MAC	Mobile air conditioning
PCM	Phase change material
RTD	Resistance temperature detector
SEM	Scanning Electron Microscopy
TES	Thermal energy storage
Symbols	
C_p	Specific heat capacity (kJ.kg^{-1}. K^{-1})
h	Latent heat of fusion (kJ. kg^{-1})
k	Thermal conductivity (W.m^{-1}. K^{-1})
R	Radius (mm)
T	Temperature (°C)
Greek symbols	
μ	Dynamic viscosity (Pa.s)
γ	Shear rate (s-1)
Subscripts	
1,2,3,4, and 5	Temperature measuring locations
bath	Bath temperature
initial	Initial temperature
l	Liquid
s	Solid

References

1. Streimikiene, D.; Balezentis, T.; Balezentien, L. Comparative assessment of road transport technologies. *Renew. Sustain. Energy Rev.* **2013**, *20*, 611–618. [CrossRef]
2. Ji, C.; Yu, M.; Wang, S.; Zhang, B.; Cong, X.; Feng, Y.; Lin, S. The optimization of on-board H2 generator control strategy and fuel consumption of an engine under the NEDC condition with start-stop system and H2 start. *Int. J. Hydrog. Energy* **2016**, *41*, 19256–19264. [CrossRef]
3. Fonseca, N.; Casanova, J.; Valdes, M. Influence of the stop/start system on CO_2 emissions of a diesel vehicle in urban traffic. *Transp. Res. Part D* **2011**, *16*, 194–200. [CrossRef]
4. Ibarra, D.; Ramirez-Mendoza, R.A.; Lopez, E.; Bustamante, R. Influence of the automotive Start/Stop system on noise emission. *Exp. Stud. Appl. Acoust.* **2015**, *100*, 55–62. [CrossRef]
5. Veerakumar, C.; Sreekumar, A. Phase change material based cold thermal energy storage: Materials, techniques and applications—A review. *Int. J. Refrig.* **2016**, *67*, 271–289. [CrossRef]
6. Rozanna, D.; Chuah, T.G.; Salmiah, A.; Choong, S.Y.; Saari, M. Fatty acids as phase change materials (PCMs) for thermal energy storage: A review. *Int. J. Green Energy* **2005**, *1*, 495–513. [CrossRef]
7. Bista, S.; Hosseini, S.E.; Owens, E.; Phillips, G. Performance improvement and energy consumption reduction in refrigeration systems using phase change material (PCM). *Appl. Therm. Eng.* **2018**, *142*, 723–735. [CrossRef]
8. Elarem, R.; Mellouli, S.; Abhilash, E.; Jemni, A. Performance analysis of a household refrigerator integrating a PCM heat exchanger. *Appl. Therm. Eng.* **2017**, *125*, 1320–1333. [CrossRef]
9. Maiorino, A.; Duca, M.G.; Mota-Babiloni, A.; Greco, A.; Aprea, C. The thermal performances of a refrigerator incorporating a phase change material. *Int. J. Refrig.* **2019**, *100*, 255–264. [CrossRef]
10. Bakhshipour, S.; Valipour, M.S.; Pahamli, Y. Parametric analysis of domestic refrigerators using PCM heat exchanger. *Int. J. Refrig.* **2017**, *83*, 1–13. [CrossRef]
11. Yamada, A.; Nishida, S.; Yokoyama, N.; Abei, J.; Danjo, T.; Florida, L.; Brodie, B.; Nagano, Y. *Cold Storage Air Conditioning System for Idle Stop Vehicle*; SAE Technical Paper 2013-01-1287; SAE International: Warrendale, PA, USA, 2013.

12. Wang, M.; Wolfe, E.; Craig, T.; Laclair, J.T.; Abdelaziz, O.; Gao, Z. *Design and Testing of a Thermal Storage System for Electric Vehicle Cabin Heating*; SAE Technical Paper 2016-01-0248; SAE International: Warrendale, PA, USA, 2013.
13. Sharma, A.; Shukla, A. Thermal cycle test of binary mixtures of some fatty acids as phase change materials for building applications. *Energy Build.* **2015**, *99*, 196–203. [CrossRef]
14. Choi, D.H.; Lee, J.; Hong, H.; Kang, Y.T. Thermal conductivity and heat transfer performance enhancement of phase change materials (PCM) containing carbon additives for heat storage application. *Int. J. Refrig.* **2014**, *42*, 112–120. [CrossRef]
15. Harish, S.; Orejon, D.; Takata, Y.; Kohno, M. Thermal conductivity enhancement of lauric acid phase change nanocomposite in solid and liquid state with single-walled carbon nanohorn inclusions. *Thermochim. Acta* **2015**, *600*, 1–6. [CrossRef]
16. Li, T.; Lee, J.H.; Wang, R.; Kang, Y.T. Enhancement of heat transfer for thermal energy storage application using stearic acid nanocomposite with multi-walled carbon nanotubes. *Energy* **2013**, *55*, 752–761. [CrossRef]
17. Yavari, F.; Fard, H.R.; Pashayi, K.; Rafiee, M.A.; Zamiri, A.; Yu, Z.Z.; Ozisik, R.; Borca-Tasciuc, T.; Koratkar, N. Enhanced thermal conductivity in a nanostructured phase change composite due to low concentration graphene additives. *J. Phys. Chem. C* **2011**, *115*, 8753–8758. [CrossRef]
18. Fan, L.; Fang, X.; Wanga, X.; Zeng, Y.; Xiao, Y.; Yu, Z.; Xuc, X.; Hua, Y.; Cen, K. Effects of various carbon nanofillers on the thermal conductivity and energy storage properties of paraffin-based nanocomposite phase change materials. *Appl. Energy* **2013**, *110*, 163–172. [CrossRef]
19. Kuila, T.; Bose, S.; Mishra, A.K.; Khanra, P.; Kim, N.H.; Lee, J.H. Chemical functionalization of graphene and its applications. *Prog. Mater. Sci.* **2012**, *57*, 1061–1105. [CrossRef]
20. Sidney, S.; Dhasan, M.L.; Selvam, C.; Harish, S. Experimental investigation of freezing and melting characteristics of graphene-based phase change nanocomposite for cold thermal energy storage applications. *Appl. Sci.* **2019**, *9*, 1099. [CrossRef]
21. Parameshwaran, R.; Deepak, K.; Saravanan, R.; Kalaiselvam, S. Preparation, thermal and rheological properties of hybrid nanocomposite phase change material for thermal energy storage. *Appl. Energy* **2014**, *115*, 320–330. [CrossRef]
22. Sathishkumar, A.; Kumaresan, V.; Velraj, R. Solidification characteristics of water based graphene nanofluid PCM in a spherical capsule for cool thermal energy storage applications. *Int. J. Refrig.* **2016**, *66*, 73–83. [CrossRef]
23. Kumaresan, V.; Velraj, R.; Das, S.K. The effect of carbon nanotubes in enhancing the thermal transport properties of PCM during solidification. *Heat Mass Transf.* **2012**, *48*, 1345–1355. [CrossRef]
24. Kumaresan, V.; Chandrasekaran, P.; Nanda, M.; Maini, A.K.; Velraj, R. Role of PCM based nanofluids for energy efficient cool thermal storage system. *Int. J. Refrig.* **2013**, *36*, 1641–1647. [CrossRef]
25. Chandrasekaran, P.; Cheralathan, M.; Kumaresan, V.; Velraj, R. Solidification behavior of water based nanofluid phase change material with a nucleating agent for cool thermal storage system. *Int. J. Refrig.* **2014**, *41*, 157–163. [CrossRef]
26. Liu, Y.; Li, X.; Hu, P.; Hu, G. Study on the supercooling degree and nucleation behavior of water based graphene oxide nanofluids PCM. *Int. J. Refrig.* **2015**, *50*, 80–86. [CrossRef]
27. Mo, S.P.; Chen, Y.; Yang, J.; Luo, X. Experimental study on solidification behavior of carbon nanotube nanofluid. *Adv. Mater. Res.* **2011**, *171*, 333–336. [CrossRef]
28. Prabakaran, R.; Kumar, J.P.N.; Lal, D.M.; Selvam, C.; Harish, S. Constrained melting of graphene-based phase change nanocomposites inside a sphere. *J. Therm. Anal. Calorim.* **2019**, 1–12. [CrossRef]
29. Prabakaran, R.; Lal, D.M.; Prabhakaran, A.; Kumar, J.K. Experimental investigations on the performance enhancement using minichannel evaporator with integrated receiver dryer condenser in an automotive air conditioning system. *Heat Transf. Eng.* **2019**, *40*, 667–678. [CrossRef]
30. Moffat, R.J. Describing the uncertainties in experimental results. *Exp. Therm. Fluid Sci.* **1998**, *1*, 3–17. [CrossRef]
31. Zheng, R.T.; Gao, J.W.; Wang, J.J.; Chen, G. Reversible temperature regulation of electrical and thermal conductivity using liquid-solid phase transitions. *Nat. Commun.* **2011**, *2*, 289. [CrossRef]
32. Harish, S.; Orejon, D.; Takata, Y.; Kohno, M. Thermal conductivity enhancement of lauric acid phase change nanocomposite with graphene nanoplatelets. *Appl. Therm. Eng.* **2015**, *80*, 205–211. [CrossRef]

33. Utomo, A.; Poth, H.; Robbins, P.T.; Pacek, A.W. Experimental and theoretical studies of thermal conductivity, viscosity and heat transfer coefficient of titania and alumina nanofluids. *Int. J. Heat Mass Transf.* **2012**, *55*, 7772–7781. [CrossRef]
34. Li, W.; Wang, Y.H.; Kong, C.C. Experimental study on melting/solidification and thermal conductivity enhancement of phase change material inside a sphere. *Int. Commun. Heat Mass Transf.* **2015**, *68*, 276–282. [CrossRef]